

The young Sun and the atmosphere and photochemistry of the early Earth

V. M. Canuto*, J. S. Levine†, T. R. Augustsson†, C. L. Imhoff‡ & M. S. Giampapa§

* NASA, Goddard Institute for Space Studies, New York, New York 10025, USA and Department of Physics, City University of New York, New York 10031, USA

† NASA, Langley Research Center, Hampton, Virginia 23665, USA

‡ Computer Sciences Corporation, Astronomy Department, Silver Springs, Maryland 20910, USA

§ Sacramento Peak Observatory, PO Box 26732, Tucson, Arizona 85726, USA

The origin and evolution of the Earth's early atmosphere depend crucially on the dissipation time t_N of the primitive solar nebula, SN. Using different theories of turbulence, we estimate that for a $0.1 M_\odot$ SN, t_N is 2.5–8.3 Myr. Because accretion times are usually much longer, we conclude that most planetary accretion must have occurred in a gas-free environment. Using new IUE data, a wavelength-dependent UV flux is constructed for the young Sun which is then used to study the photochemistry and concentrations of O, O₂, O₃, OH, H, HCO and formaldehyde H₂CO in the Earth's early prebiological atmosphere.

THERE is convincing observational evidence that the placent interstellar medium (ISM) from which the Solar System originated was a dense molecular cloud^{1,2}. In fact, the recent evidence of the presence of short-lived nuclei in meteorites² requires that the free-fall time scale for gravitational collapse (t_{ff}) be less than or comparable with the mean lifetime of ²⁶Al (10^6 yr), that is $t_{ff} \leq 4 \times 10^7 / \sqrt{n_H} < 10^6$ yr, which requires² $n_H > 10^3 \text{ cm}^{-3}$, a value typical of molecular clouds. As molecular clouds are observed to be a major feature in our Galaxy, they constitute a reliable starting point for the processes that will eventually lead to the formation of stars and planetary systems³. A detailed analysis of the events that take place in such clouds, after an external agent has caused them to become unstable, has been worked out for a large variety of initial conditions^{4,5}. Typically: $M/M_\odot = 10^4$, $\rho = 1.7 \times 10^{-23} \text{ g cm}^{-3}$, $T = 75 \text{ K}$, $R = 6.6 \times 10^{19} \text{ cm}$, $\Omega = 10^{-15} \text{ rad s}^{-1}$, and $J/M = 1.75 \times 10^{24} \text{ cm}^2 \text{ s}^{-1}$. Since T-Tauri stars have $J/M = 10^{17} - 10^{18} \text{ cm}^2 \text{ s}^{-1}$, a major effort has been dedicated to understand how to achieve a reduction of about 6 orders of magnitude in the value of J/M . The analysis indicates that the J/M reduction may be best achieved through a hierarchy of collapse and fragmentation and that the process yields binary fragments, a reassuring result in view of the preponderance of binary star systems. The most relevant result of these computations is that the fragments form with masses larger than the local Jeans masses, ensuring their continuous collapse, thus placing, the hierarchical fragmentation model on firm foundations⁶.

Recent work^{6,7} has, however, indicated difficulties with the previous scenario. Study of the collapse of a dark cloud ($M = 50 M_\odot$, $T = 10 \text{ K}$, $R = 2 \times 10^{18} \text{ cm}$, $\Omega = 3 \times 10^{-14} \text{ rad s}^{-1}$, $J/M = 4 \times 10^{22} \text{ cm}^2 \text{ s}^{-1}$) indicates that a binary system is first formed with $M/M_\odot = 8$, each of the two fragment dividing further into a triple system with $M/M_\odot = 2$, $R = 2 \times 10^{15} \text{ cm}$, $J/M = 10^{20} \text{ cm}^2 \text{ s}^{-1}$. The dynamics of each triple system indicates⁸ that one object will be ejected in a time scale of $t \approx 10^5$ yr, thus isolating one of the three partners which may then be considered a candidate for a massive primitive solar nebula as demanded in ref. 9. This sequence of events may, however, not be the true endpoint of the fragmentation process. A recent study⁷ of the fate of the $2M_\odot$ ejected body indicates that it will further fragment into a multiple system, a process that will stop only at $M < 0.1M_\odot$. These results show that fragmentation is not a self-regulating mechanism until one reaches $M \sim 10^{-2}M_\odot$, in agreement with an earlier analytic result¹⁰ on opacity limited fragmentation. It has been suggested¹¹ that turbulence rather than simple fragmentation may be the relevant mechanism at work in star formation. If so, the resulting mass interval is $5 \times 10^{-2} \leq M/M_\odot \leq 1$, thus suggesting a solar nebula less massive than that of ref. 9 (see also ref. 12).

Protostellar evolution—UV spectrum

Observationally, the pre-main-sequence stars appear to pass through three phases of evolution. While extremely young, the protostars are detected primarily at IR wavelengths. This phase is thought to correspond with the accretion of the protostellar core, obscured beyond a shroud of dust. Theoretical models¹³ indicate that a $1M_\odot$ star will remain in this early stage for 10^5 yr.

The second phase, characterized by the T-Tauri stars, begins as the protostars become visible. By this time, relatively small amount of gas and dust accompany the star; the stellar photosphere and bright chromosphere may be seen. The termination of this phase may be estimated from the maximum observed ages of the stars. Examinations of several associations, using member hot stars of known ages and stability arguments, indicate ages of 3–5 Myr (refs 14, 15). If the T-Tauri stage corresponds to the fully convective phase of pre-main-sequence evolution (vertical portion of the tracks of Fig. 1), then theoretical predictions may be used¹⁶: 2 Myr for a $2M_\odot$ star, 12 Myr for a $1M_\odot$ star, and 40 Myr for a $0.7M_\odot$ star. The ages for several T-Tauri stars in several young associations and clusters have been estimated from their HR diagram¹⁷. Figure 1 shows three evolutionary tracks, superimposed on data obtained for stars in Taurus–Auriga and Orion¹⁷, indicating ages from 10^5 to 10^7 yr. Considering that the stars are variable, rotate, possess magnetic fields and lose mass, complications with which the theory cannot yet deal completely, the overall agreement among ages derived by all these methods is good. Thus we conclude that, for a solar mass star, the T-Tauri stage of pre-main-sequence evolution begins when the star is $\sim 10^5$ yr old and lasts until it is ~ 6 –12 Myr old.

The phase following the T-Tauri stars, the radiative phase, although it comprises over 80% of the time required for the star to evolve to the main sequence, is not as well-defined observationally. Herbig¹⁸ postulated the probable characteristics of the post T-Tauri star. Unexpectedly, a few such stars have been found through X-ray detection by the Einstein satellite^{19,20}. The post T-Tauri stars exhibit the characteristics expected for protostars which are more evolved than the T-Tauri stars. However, no clear difference in ages has yet been established²¹. Thus clear examples of solar mass protostars with ages of 10–50 Myr are as yet lacking.

The Sun is a relatively normal star of moderate mass, temperature and luminosity; it is very reasonable to assume that it passed through these three phases of pre-main-sequence evolution. Therefore, we can use UV observations of pre-main-sequence stars to represent the UV spectrum of the youthful Sun. Several such stars have been observed with the International Ultraviolet Explorer (IUE)^{22–26}. Virtually all of the data

have been obtained for the brighter T-Tauri stars. Thus we use IUE spectra of three of the best studied T-Tauri stars to represent the probable solar UV spectrum at roughly an age of 1–10 Myr. We have drawn on comprehensive data (acquired by two of us) for three bright T-Tauri stars, SU Aurigae, RW Aurigae, and T Tauri (prototype of the class). The three stars form a reasonable sample of the heterogeneous class, representing a range of T-Tauri characteristics. Fourteen low-resolution IUE spectra of the three stars were averaged to produce a composite T-Tauri UV spectrum. The composite spectrum lacks information at the short wavelength end concerning the very strong hydrogen Ly α line because of geocoronal Ly α emission contamination. A weak stellar Ly α emission feature can be seen in the spectrum of RW Aurigae, superimposed on the geocoronal feature. A rough estimate of the flux indicates that the Ly α line in RW Aur is about 1/10 as strong as its hydrogen Balmer- α emission line²⁷. Thus we have estimated the Ly α fluxes for the three T-Tauri stars as 0.1 times their respective Balmer- α fluxes. These estimates are consistent with the non-detections in SU Aur and T Tau. To complete the composite T-Tauri spectrum we have used published visual fluxes of these stars²⁷. Small gaps in the UV and visual data were interpolated, as no strong emission lines are expected at those wavelengths. The mean spectrum of the visual spectra of the three stars was formed and reduced to the flux intercepted at a distance of 1 AU. A conservative correction for dust extinction corresponding to $A_v = 0.5$ mag was made. The resulting T-Tauri spectrum normalized to the present solar value is presented in Fig. 2. Three strong emission lines are notable: Ly α (121 nm), Mg II (280 nm) and Balmer α (656 nm). The greater luminosity of the average T-Tauri star may be seen at all wavelengths. However, the ratio is a strong function of wavelength: at the shortest wavelengths to which the photochemical processes are most sensitive, a young star is brighter than the present Sun by $>10^4$.

Thus, the use of this observationally determined UV spectrum rather than a wavelength-independent approximation²⁸ constitutes a significant improvement to the input for modelling the photochemistry of the early atmosphere.

It might be argued that the extreme level of UV emission seen in the T-Tauri stars does not characterize the solar UV spectrum of the Sun's subsequent evolution towards the main sequence. The lack of known 'old' post T-Tauri stars does not allow us a direct observational test. However, Bøsegaard and Simon²⁹ have studied the changes in the UV emission lines originating in the stellar chromosphere (corresponding to $\lambda < 1,900$ Å) with age for several young main sequence stars. The line fluxes, normalized to stellar surface areas, fall off roughly as $t^{-1/2}$. We have used this result to estimate how the emission line flux decreases with time after the T-Tauri phase²⁸. We find that, even after the Sun has reached the main sequence, its far-UV luminosity is still 10^2 times the present value. The slow decrease in the UV flux means that the results derived here for the T-Tauri phase are largely applicable, with moderate down-scaling, to the later stages of the Sun's pre-main-sequence evolution.

Earth formation—solar nebula dissipation

The accretion process that led to the formation of the earth from grains, dust and gas has been studied by several authors^{12,30–36}. (For a detailed review, see ref. 32.) While early estimates by Schmidt³⁰ resulted in an accretion time $t_A \approx 250$ Myr, all recent analyses³² yield considerably lower values, that is $23 \leq t_A \leq 88$ Myr. These results assume that accretion occurred in the absence of gas³². In the presence of gas^{32–35}, t_A decreases to ~ 10 Myr, and a massive atmosphere ($\sim 10^4$ times the present one or the one corresponding to the gas-free situation) results. Since the two models lead to very different conclusions for the Earth's atmosphere, it is important to analyse their basic ingredients. A critical role is played by t_N , the dissipation time of the solar nebula, whose value depends in most models considered thus far, on the turbulent viscosity

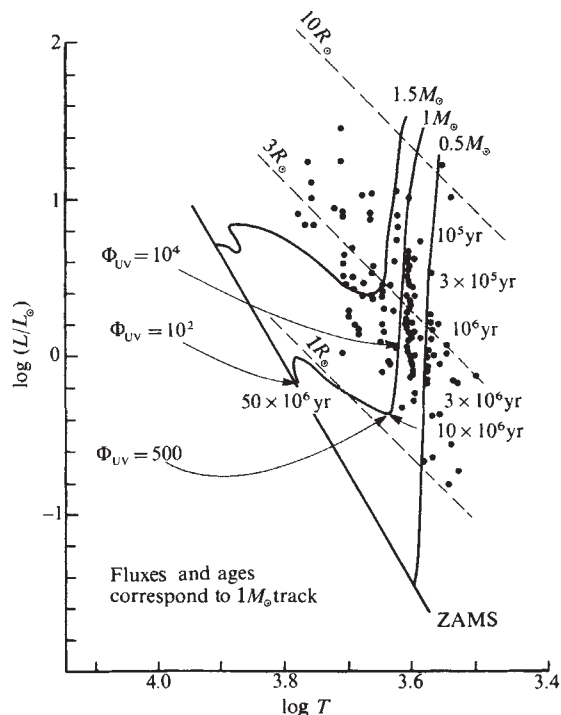


Fig. 1 The pre-main-sequence evolution of $0.5M_{\odot}$, $1M_{\odot}$ and $1.5M_{\odot}$ stars. ●, Observational data¹⁷. The increase in the UV flux Φ_{UV} (measured in terms of its present value) as well as the ages for $1M_{\odot}$ star have been indicated. It is seen that at $t = 10^7$ yr, corresponding to the end of the T-Tauri phase, the UV flux was 500 times stronger than today.

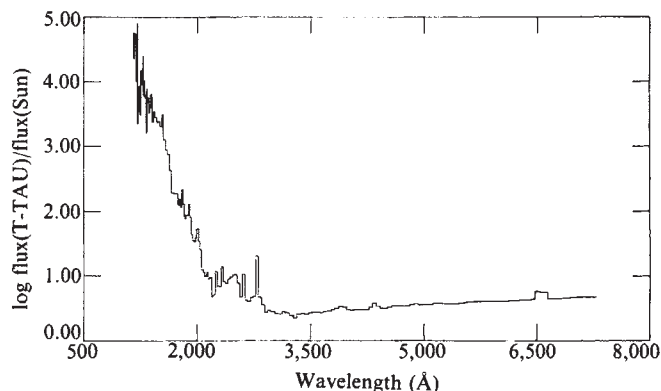


Fig. 2 The composite UV flux (normalized to its present value) as derived using 14 spectra of three T-Tauri stars. In the region of importance to photochemical processes, the UV flux is 10^4 greater than its present value.

$\nu_t = \xi l v_t$ (where l_t and v_t are typical lengths and velocities of the turbulent motion). A detailed analysis³⁷ leads to the following dependence of t_N on ξ

$$t_N = \frac{A}{4\xi} \text{ Myr} \quad (1)$$

where $A = (M_N/10^{-1}M_{\odot})^{1.37} (X/50 \text{ AU})^{-1.37} (V_w \dot{M}_w/2 \times 10^{26})^{-1.33}$. Here, M_N is the mass of the solar nebula, X its extension, V_w the solar wind and \dot{M}_w the rate of mass loss^{38–41}. In the absence of a direct estimate of ξ , one can only say that³³

$$10^{-3} \leq \xi \leq 1/3 \quad (2)$$

a result arrived at as follows. In the standard treatment of a turbulent fluid, one envisages three regions characterized by different sizes of the eddies there contained. In the first region, the eddy sizes l are comparable with L , the size of the system itself. In this case one writes $\nu = \xi_L v l$, where ξ_L is the inverse of the Reynolds number Re which, for turbulence to set in, must be $>10^3$, and so $\xi_L < 10^{-3}$, yielding the lower limit in

equation (2). At the other end of the spectrum, the eddies are sufficiently small for molecular forces to dominate, and so $\nu = \xi_m \nu_l$, where $\xi_m = 1/3$, thus yielding the upper unit in equation (2).

In the intermediate size region, containing all the turbulent phenomena, $\nu_i = \xi l_i \nu_l$ and ξ must be computed from first principles. Using the Heisenberg–Weizsacker's theory of turbulence⁴², one has

$$\nu_i(k) = \gamma \int_k^\infty \left(\frac{F(k)}{k^3} \right)^{1/2} dk, \quad (3)$$

$$v_i^2 = \int_k^\infty F(k) dk, \quad l_i = \pi/k$$

where $F(k)$ is the spectral-energy distribution function solution of the dynamical equations governing turbulence. We have computed ξ using:

(1) Kolmogoroff spectrum⁴², $F(k) \sim k^{-5/3}$. In this case

$$\xi = \frac{\gamma}{\pi} \sqrt{\frac{3}{8}} = 0.06, \quad \gamma = 1/3 \quad (4)$$

(2) The Steward–Townsend⁴² experimental spectrum $F(k) \sim k^{-\alpha \ln k}$. We obtain

$$\xi = \frac{\gamma q}{\pi} \sqrt{\frac{2}{\alpha}} \frac{1 - \Phi(x)}{\{1 - \Phi(y)\}^{1/2}} \quad (5)$$

where $x\sqrt{2} = \alpha \ln q + 0.5\alpha^{-1}$, $y = \alpha \ln q - 0.5\alpha^{-1}$, $q = k/k_0 = L/l$. We solved equation (5) numerically. For a wide range of parameters, the resulting values of ξ are

$$0.03 \leq \xi < 0.08 \quad (6)$$

(3) The theory of convective turbulence developed in ref. 43 and valid for $R\sigma \ll 1$, where R is the Rayleigh number and σ the Prandtl number. Since $F(k)$ cannot be given in closed analytical form, the evaluation of ξ was done numerically. For the range $10^{-7} < \delta < 10^{-1}$ of $\delta = 8\pi^4/R$, the result is

$$0.03 < \xi < 0.07 \quad (7a)$$

(4) We have extended the theory of ref. 43 to the case $R\sigma \gg 1$. Because the entire analysis must be done numerically, we report only the final result, that is

$$0.06 \leq \xi \leq 0.07 \quad (7b)$$

(5) The theory of convective turbulence developed by one of us (V.M.C., in collaboration with I. Goldman) in which the Heisenberg expression (3) for ν_i is changed to the integral over k of the ratio $F(k)/n(k)$, where $n(k)$ is the growth rate of the laminar modes⁴³. The result is $(H^2 = h/2\lambda q^2, h = (1 + \lambda^2 q^4)^{1/2} - \lambda q^2, C_\lambda^2 = (1 + \lambda^2)^{1/2} + \lambda)$

$$\xi = \left(\frac{\gamma_* C_\lambda}{\pi^2} \right)^{1/2} q (2\lambda)^{1/4} \frac{(1 + H^2)^{1/2} - 1}{(H - \lg^{-1} H)^{1/2}} \quad (8)$$

where $\lambda^2 = 2\pi^4/R\sigma$ and $\gamma_* = 2/15$ (ref. 44). For $\lambda \gg 1$

$$\xi = \left(\frac{3\gamma_*}{4\pi^2} \right)^{1/2} = 0.1 \quad (9)$$

Using these results, as well as that of ref. 44, i.e. $\xi = 0.05$, we conclude that for $A = 1$

$$t_N = 2.5\text{--}8.3 \text{ Myr} \quad (10)$$

A similar result, $t_N \sim 10$ Myr, has also been obtained in ref. 45. Note that the upper limit of t_N closely corresponds to the point where the T-Tauri phase (vertical part of the $1M_\odot$ track, Fig. 1) ends. Furthermore, because either value of t_N is smaller than the values³² of t_A , it seems unlikely that gas might have influenced accretion to the point of producing a massive H_2 atmosphere. Because the quoted values of t_A , ranging from 10 Myr to 23–88 Myr correspond to extreme assumptions as far as the gas is concerned, our result suggesting a gradual dispersion of the gas while the Earth was accreting, would in principle require a new evaluation of t_A with a time-decreasing gas density. However, for the present purposes, it is sufficient to take an average of the previous values. If we take $t_A = 50$ Myr, we would conclude that the SN gas was present only for 10% of t_A , and that most of the accretion occurred while the Sun was moving

along the radiative track stage of Fig. 1. When the Earth was accreted, the UV flux was therefore about 10^2 times larger than its present value, large enough to influence the photochemistry of its atmosphere significantly.

Origin of the atmosphere

Having concluded that the SN was an unlikely contributor to the Earth's atmosphere, one may consider the following potential contributors⁴⁶: (1) collision with comets⁴⁷, (2) volatilization of impacting material and (3) outgassing. One may distinguish two periods of outgassing⁴⁸. While the accretion energy due to impact was in principle sufficient to melt the entire Earth, this may not have occurred, since a fully melted Earth would have expelled all volatiles, whilst it is known that ^3He is still degassed today. Accretional heating may have produced partial melting including Fe alloys that migrated towards the centre forming ultimately the Earth's core. The time scales for the core formation discussed in the past ($\approx 10^9$ yr) have been shown to be too long. The conclusion is that the core formed contemporaneously with the accretion of the Earth itself, that is in $\approx 10^7$ yr (ref. 48). During this period, two sources of volatiles therefore acted simultaneously, the outgassing caused by the impacting material that stirred the mantle and the impacting meteorites. Because volatiles are bound in these meteorites, the energy retained as heat on impact would be sufficient to vaporize the volatile species, releasing them so as to form an atmosphere. As stated in ref. 49 this conclusion seems unavoidable: the formation only of a solid body with the subsequent outgassing seems an artificial division of events which more naturally should be thought of as having occurred simultaneously. As the embryonic Earth continued to grow, the impact velocities increased until vaporization of the impacting material occurred. Non-volatile solids so vaporized cooled and condensed onto the surface. Volatiles such as H_2O , CO_2 , N_2 , and noble gases probably remained in the atmosphere. Calculations⁵⁰ indicate that this process occurs for impact velocities $> 5 \text{ km s}^{-1}$, which in the case of the Earth was achieved⁵¹ when the radius was 50% of its present value, that is before $\sim 10^6$ yr (Fig. 10 of ref. 52).

The chemical composition of this atmosphere depends critically on complex chemical reactions between the infalling vaporized gas, the outgassed volatiles and other elements, particularly Fe (G. W. Wetherill, personal communication). In the specific impact originated atmosphere studied in ref. 50, the partial pressure of water was estimated to be $P_{H_2O} \approx 0.01$ bar. The fate of atmospheric CO_2 is difficult to quantify and experiments by Ahrens and collaborators (D. J. Stevenson, personal communication) are expected to shed light on this point, because carbonate growth may have removed a great deal of CO_2 during the time scale of the Earth's accretion. The first phase of outgassing, together with an impact-originated atmosphere, lasted a period of time not greatly different from the accretion time itself, at the end of which the Earth entered a period in which accretion is over, the mantle solid and the core fully formed⁴⁸. Such a period is characterized by a large 'mass flux' which transports large masses of the mantle to the surface region, thus making them available for the second period of outgassing. Because the length of this period is difficult to estimate, the following argument can be made⁵³. The abundance of $^{129}\text{Xe}/^{130}\text{Xe}$ in the atmosphere is smaller than that in the solid Earth, the latter being due to enrichment caused by the decay of ^{129}I to ^{129}Xe . If the outgassing took much longer than a few lifetimes of ^{129}I (17 Myr), at the end of it there would have been no ^{129}Xe left and both the atmospheric and the terrestrial ^{129}Xe should have been equally abundant. As this is not the case, the separation of the ^{129}Xe from the Earth (outgassing), must have occurred while ^{129}I was still present, that is within a few ^{129}I lifetimes, say 50 Myr. (However, as Wetherill has noted, the argument is also consistent with no outgassing of the Earth at all, all the atmospheric ^{129}Xe having perhaps been deposited in the atmosphere by impact.)

We therefore conclude that the entire set of phenomena, (1) collapse of the nebula, (2) accretion of the Earth, (3) dissipation

of the nebular remnant, (4) formation of the Earth's core, (5) formation of an atmosphere by impact volatiles plus outgassing and (6) contribution to the atmosphere by the second outgassing period, may have occurred within 50–100 Myr, corresponding to the time when the Sun entered the main sequence (Fig. 1).

On the basis of the previous discussion, for our photochemical calculations we have assumed a background composition of the palaeoatmosphere consistent with both the impact and outgassing scenarios. We adopt an H₂O vapour partial pressure of 0.01 bar, as from ref. 50. The H₂O mixing ratio varies from 1.2×10^{-2} at the surface to 4.6×10^{-7} at the tropopause. Above it, the distribution of H₂O vapour is calculated using a continuity/transport equation for H₂O. Because of the lack of firm experimental evidence concerning the rate of removal of atmospheric CO₂ due to carbonate growth, the level of CO₂ cannot be uniquely determined. We have therefore performed our photochemical calculations for two representative values: CO₂ = 1 (the pre-industrial level of 280 p.p.m.v.) and CO₂ = 100 times that value. Higher values of CO₂ seem improbable⁴⁵. Furthermore, we have adopted 0.8 bar of N₂, a chemically inert gas that participates in the chemical reactions only as a third

body. We have also added the trace gases H₂ and CO. Calculations were performed for the two values of the surface mixing ratios H₂, namely 17 p.p.m.v. and 10^{-3} (refs 54, 55). The surface flux of CO was taken to be 2×10^8 (molecules cm⁻² s⁻¹) which corresponds to a surface mixing ratio of parts per billion by volume. CH₄ and NH₃ were not included for reasons explained elsewhere^{56,57}.

Photochemistry of oxygen, ozone and formaldehyde

Studies dealing with the origin and evolution of life⁵⁸ have indicated that formaldehyde, H₂CO, was a key molecule in the process of chemical evolution, that is the formation of complex organic molecules. Today, H₂CO is a trace species produced by the methane oxidation chain with the precursor CH₄ being provided by biogenic activity. Because the lifetime of CH₄ in the prebiological atmosphere is extremely short^{56,57} due to photochemical destruction, the question then arises as to how to produce H₂CO in the absence of a steady source of CH₄. A prebiological photochemical source for H₂CO has been suggested⁵⁵. As we shall show below, it is sensitive to the UV flux

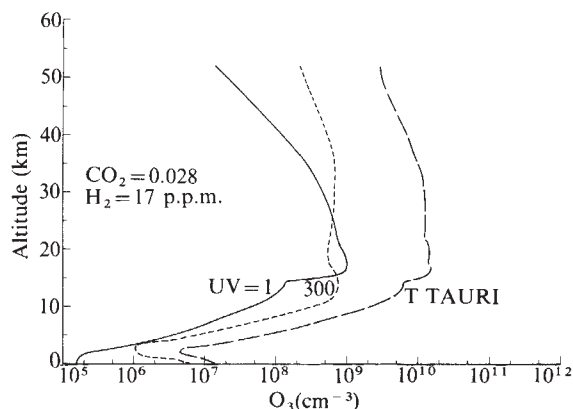


Fig. 3 The ozone profile. The solid curve (UV = 1) corresponds to the present UV flux. The curve labelled UV = 300 corresponds to a wavelength-independent increase by a factor of 300. The curve labelled T Tauri corresponds to the use of the flux of Fig. 2. A substantial increase in the amount of O₃ can be seen (see Tables 3, 4).

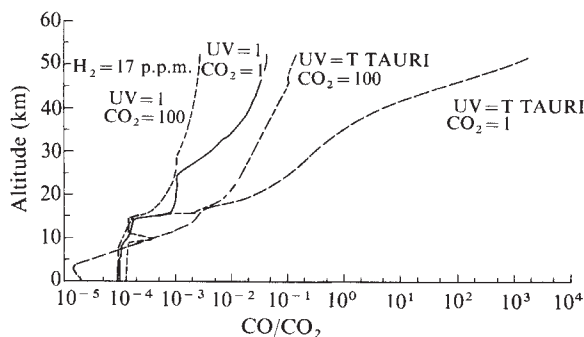


Fig. 4 The vertical profile of the ratio CO/CO₂ of interest to laboratory simulation experiments for the formation of organic molecules⁶¹. It can be seen that only with an enhanced UV flux does one obtain CO/CO₂ ≥ 1.

Table 1 Solar energy flux averaged over the Earth during T-Tauri phase (numbers in parentheses correspond to present day values)

Source	Energy (cal cm ⁻² yr ⁻¹)
Total radiation	4.6×10^6 (0.26×10^6)
UV light	
< 3,000 Å	2.4×10^4 (0.34×10^4)
< 2,500 Å	9.9×10^3 (0.56×10^3)
< 2,000 Å	5.0×10^3 (40)
< 1,500 Å	2.2×10^3 (1.7)

Table 2 Photochemical and chemical reactions

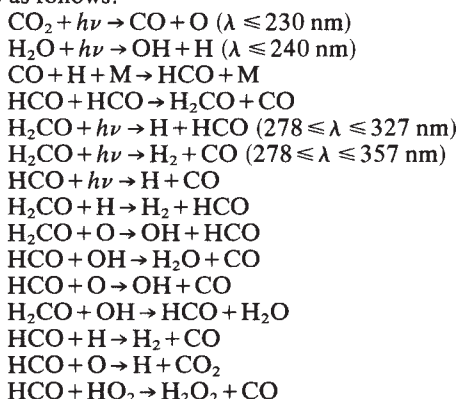
Reaction no.	Reaction	Rate constant* (s ⁻¹ , cm ³ s ⁻¹ or cm ⁶ s ⁻¹)	
J1	O ₂ + hν → O + O	4.7×10^{-10}	6.3×10^{-9}
J2	O ₃ + hν → O + O ₂	2.2×10^{-4}	8.5×10^{-4}
J3	O ₃ + hν → O(¹ D) + O ₂	4.4×10^{-3}	2.8×10^{-2}
J4	H ₂ O + hν → OH + H	1.1×10^{-14}	5.1×10^{-13}
J5	H ₂ O ₂ + hν → OH + OH	5.3×10^{-5}	4.4×10^{-4}
J6	H ₂ CO + hν → H + HCO	4.8×10^{-5}	1.6×10^{-4}
J7	H ₂ CO + hν → H ₂ + CO	4.9×10^{-5}	1.4×10^{-4}
J8	CO ₂ + hν → CO + O	1.3×10^{-12}	6.3×10^{-11}
J9	HCO + hν → H + CO	1.3×10^{-2}	5.8×10^{-2}
1	O + O ₂ + M → O ₃ + M	1.1×10^{-34}	exp (510/T)
2	O + O ₃ → 2O ₂	1.5×10^{-11}	exp (-2,218/T)
3	O(¹ D) + O ₂ → O + O ₂	3.2×10^{-11}	exp (67/T)
4	O(¹ D) + N ₂ → O + N ₂	2.0×10^{-11}	exp (107/T)
5	H ₂ O + O(¹ D) → 2OH	2.3×10^{-10}	
6	H + O ₂ + M → HO ₂ + M	2.1×10^{-32}	exp (290/T)
7	H + O ₃ → OH + O ₂	1.4×10^{-10}	exp (-470/T)
8	OH + O → H + O ₂	4.0×10^{-11}	
9	OH + O ₃ → HO ₂ + O ₂	1.6×10^{-12}	exp (-940/T)
10	OH + OH → H ₂ O + O	1.0×10^{-12}	exp (-500/T)
11	HO ₂ + O → OH + O ₂	3.5×10^{-11}	
12	HO ₂ + O ₃ → OH + 2O ₂	1.1×10^{-14}	exp (-580/T)
13	HO ₂ + OH → H ₂ O + O ₂	4.0×10^{-11}	
14	HO ₂ + HO ₂ → H ₂ O ₂ + O ₂	2.5×10^{-12}	
15	H ₂ O ₂ + OH → HO ₂ + H ₂ O	1.0×10^{-11}	exp (-750/T)
16	O(¹ D) + H ₂ → OH + H	9.9×10^{-11}	
17	OH + OH + M → H ₂ O ₂ + M	†	
18	H ₂ O ₂ + O → OH + HO ₂	2.8×10^{-12}	exp (-2,125/T)
19	H ₂ + OH → H ₂ O + H	1.2×10^{-11}	exp (-2,200/T)
20	H ₂ CO + OH → HCO + H ₂ O	1.7×10^{-11}	exp (-100/T)
21	H ₂ CO + O → OH + HCO	2.8×10^{-11}	exp (-1,540/T)
22	HCO + O ₂ → CO + HO ₂	5.0×10^{-12}	
23	CO + OH → H + CO ₂	†	
24	O + O + M → O ₂ + M	2.8×10^{-34}	exp (710/T)
25	H + H + M → H ₂ + M	8.3×10^{-33}	
26	H ₂ + O → OH + H	3.0×10^{-14}	exp (-4,480/T)
27	H + HO ₂ → O ₂ + H ₂	4.7×10^{-11}	(×0.29)
28	H + HO ₂ → H ₂ O + O	4.7×10^{-11}	(×0.02)
29	H + HO ₂ → OH + OH	4.7×10^{-11}	(×0.69)
30	H + CO + M → HCO + M	2.0×10^{-33}	exp (-850/T)
31	H + HCO → H ₂ + CO	3.0×10^{-10}	
32	HCO + HCO → H ₂ CO + CO	6.3×10^{-11}	
33	OH + HCO → H ₂ O + CO	5.0×10^{-11}	
34	O + HCO → H + CO ₂	1.0×10^{-10}	
35	O + HCO → OH + CO	1.0×10^{-10}	
36	HO ₂ + HCO → H ₂ O ₂ + CO	1.0×10^{-11}	
37	H ₂ CO + H → H ₂ + HCO	2.8×10^{-11}	exp (-1,540/T)
38	H ₂ CO and H ₂ O ₂ rainout	1.0×10^{-6}	s ⁻¹

* Photolysis rates (s⁻¹) for H₂ = 17 p.p.m.v. are given for UV = 1 (first value) and UV = T-Tauri phase.

† See JPL Publ. 82-57 (1982).

and to the abundances of CO₂ and H₂. The considerable increase of UV radiation suggested by the IUE data on young Sun may therefore alter the production rate of H₂CO estimated earlier⁵⁵, a value of great interest because sufficient for polymerization purposes.

The production and destruction reactions suggested in ref. 55 are as follows:



These reactions were added to the one-dimensional photochemical model described in ref. 57 and used in ref. 28. The scheme was modified by eliminating the nitrogen and chlorine species, after it was found that they were irrelevant to the H₂CO photochemistry. The present version of the model contains 10 photochemical processes and 37 chemical reactions listed in Table 2. By simultaneously solving the coupled species continuity/transport equations, the surface concentrations and vertical profiles (up to 53.5 km) of the following species were computed: O, O₂, O₃, OH, H, HCO, H₂CO, CO, CO₂, H₂O,

Table 3 Surface concentration of several species (cm⁻³) as a function of UV flux and CO₂ and H₂ level

Species	UV = 1		UV = T-Tauri phase	
	CO ₂ = 1	CO ₂ = 100	CO ₂ = 1	CO ₂ = 100
H₂ = 17 p.p.m.				
O	8.95 (6)	4.47 (7)	4.92 (8)	1.96 (9)
O ₂	2.72 (5)	1.36 (9)	2.33 (7)	1.29 (10)
O ₃	5.66	1.69 (5)	2.20 (3)	1.46 (7)
OH	4.13 (3)	1.51 (4)	2.28 (5)	6.66 (5)
CO	5.09 (11)	7.86 (13)	1.10 (11)	5.16 (13)
H	3.24 (7)	4.09 (6)	1.36 (9)	1.28 (8)
HCO	1.39 (6)	2.06 (7)	5.58 (5)	2.50 (7)
H ₂ CO	1.62 (6)	2.65 (8)	3.38 (4)	7.17 (7)
CO/CO ₂	9.02 (-5)	1.39 (-4)	1.95 (-5)	9.15 (-5)
H₂ = 10⁻³ p.p.m.				
O	2.10 (5)	6.57 (6)	9.49 (6)	1.44 (8)
O ₂	1.87 (2)	1.20 (4)	6.12 (4)	1.99 (6)
O ₃	1.07 (-4)	2.21 (-1)	2.18 (-1)	1.15 (2)
OH	7.64 (1)	2.60 (2)	3.67 (3)	1.45 (4)
CO	3.09 (13)	3.63 (15)	2.66 (13)	2.37 (15)
H	3.46 (6)	2.32 (5)	4.34 (7)	8.60 (6)
HCO	1.50 (7)	7.95 (7)	3.26 (7)	3.55 (8)
H ₂ CO	4.14 (8)	4.12 (9)	3.79 (8)	2.43 (10)
CO/CO ₂	5.48 (-3)	6.44 (-3)	4.72 (-3)	4.20 (-3)

Table 4 Column densities of O₃ and H₂CO (molecules cm⁻²)

O ₃	UV = 1		UV = T-Tauri phase	
	CO ₂ = 1	CO ₂ = 100	CO ₂ = 1	CO ₂ = 100
H ₂ = 17 p.p.m.v.	3.3 (12)	1.5 (15)	7.4 (15)	4.05 (16)
H ₂ = 10 ⁻³	2.1 (11)	1.3 (14)	6.5 (14)	2.01 (15)
H₂CO				
H ₂ = 17 p.p.m.v.	5.4 (11)	7.34 (13)	5.9 (9)	5.45 (13)
H ₂ = 10 ⁻³	8.6 (14)	2.02 (15)	3.7 (14)	1.1 (16)

H₂, HO₂ and H₂O₂ using the UV flux of Fig. 2 to initiate photochemical processes. Water soluble species (such as H₂CO and H₂O₂) are lost by rainout with a rainout coefficient of 10⁻⁶ s⁻¹ (11.6 days), as derived from both theoretical calculations and direct measurements of the rainout lifetime of water soluble NH₃ (ref. 59). Calculated surface concentrations of the species of interest are presented in Table 3. The column densities of H₂CO and O₃ versus UV flux are presented in Table 4. Finally, the surface production, losses due to photochemistry/chemistry and rainout and the rainout rates for H₂CO are presented in Table 5.

Results

The dissipation time scale of the SN presented here, equation (10), suggests that accretion probably occurred mostly in a gas-free environment. This, together with previous results, suggest that Earth accretion and the formation of an atmosphere (due to impact and first phase of outgassing), occurred within the interval of time it took the Sun to arrive at the main sequence. During this period, the UV flux was at least 100 times larger than its present value.

The pre-main-sequence solar UV flux was determined by using observational IUE data on the T-Tauri stars. Figure 2 shows the strong wavelength dependence of the increase in the UV flux. (Present solar fluxes were taken from ref. 60.) In Table 1, we present the solar energy flux during the T-Tauri phase as averaged over the Earth. While the total radiation is ~18 times larger than its present value, the UV fluxes are increased up to 10⁴.

Our results show that the increment in the surface concentration and the vertical profile of O₂ determined in ref. 28 are not changed. As we see from Table 3, the O₂ mixing ratio increases up to 10⁴-10⁵ times, depending on the value of H₂. Furthermore, O₂ increases as the CO₂ and UV fluxes increase, as expected.

While for O₂ the quantity of interest is the surface concentration, for ozone the total column density is perhaps more relevant due to its ability to absorb UV radiation. Such a distribution turns out to be substantially altered by the use of a λ-dependent UV flux, compared with the λ-independent treatment of ref. 28. The results of Fig. 3 and Tables 3 and 4 indicate that there has been an increase in the ozone column density of 1-3 orders of magnitude.

Both O and OH radicals are seen to increase by an order of magnitude when either CO₂ or the UV flux are increased.

The CO/CO₂ ratio is a particularly interesting quantity in view of a recent laboratory experiment⁶¹ indicating that a mixture of H₂O and CO, once irradiated with UV radiation, yields a large array of organic molecules relevant to the origin of life. In the absence of CO, irradiation of CO₂ yields no organics. The profile of the CO/CO₂ ratio is presented in Fig. 4 for H₂ = 17 p.p.m., corresponding to the minimum calculated ratio. It is seen that at high altitudes the ratio is still much smaller

Table 5 Surface production and loss rates for H₂CO as a function of UV flux and CO₂ level (H₂ = 17 p.p.m.v.)

Reaction	Reaction rate (molecules cm ⁻³ s ⁻¹)			
	UV = 1		UV = T Tauri	
	CO ₂ = 1	CO ₂ = 100	CO ₂ = 1	CO ₂ = 100
1. Production				
HCO + HCO → H ₂ CO + CO	1.22 (2)	2.67 (4)	1.97 (1)	3.93 (4)
2. Loss due to photochemistry/chemistry				
H ₂ CO + hν → H + HCO	7.75 (1)	1.26 (4)	5.35 (0)	1.05 (4)
H ₂ CO + hν → H ₂ + CO	7.97 (1)	1.30 (4)	4.84 (0)	9.86 (3)
H ₂ CO + H → H ₂ + HCO	7.03 (0)	1.45 (2)	6.16 (0)	1.22 (3)
H ₂ CO + OH → HCO + H ₂ O	8.04 (-2)	4.81 (1)	9.26 (-2)	5.74 (2)
H ₂ CO + O → OH + HCO	1.94 (0)	1.58 (3)	2.22 (0)	1.88 (4)
Total	1.66 (2)	2.74 (4)	1.87 (1)	4.10 (4)
3. Loss due to rainout				
	1.62	2.65 (2)	3.38 (-2)	7.17 (1)
4. Rain-out rate				
H ₂ = 17 p.p.m.v.	5.5 (5)	7.34 (7)	5.98 (3)	5.45 (7)
H ₂ = 10 ⁻³ p.p.m.v.	8.6 (8)	2.02 (9)	3.7 (8)	1.07 (10)

than unity if the flux is unity UV and that an increase of CO₂ makes the situation only worse, as expected. If, however, the UV flux is increased as seen from Fig. 2, the situation changes radically, yielding a ratio of the order of unity or even larger at high altitudes, where the gas reactions simulated in ref. 61 are thought to occur. The increase of the UV flux has therefore distinctly improved the situation, as far as the CO/CO₂ ratio is concerned.

The value for H₂CO computed in ref. 55 and corresponding to UV = 1 and CO₂ = 1 is here well reproduced within the uncertainties due to different photochemical models and numerical schemes. Our results indicate that the concentration of H₂CO is extremely sensitive (up to four orders of magnitude) to the abundance of H₂. Column densities are presented in Table 4. Perhaps the most interesting way of expressing the results concerning H₂CO is by way of Table 5, which gives the surface production and destruction rates. We also list the loss rates, two kinds of which are of interest. The first, representing the combined action of chemistry/photochemistry, represents a real destruction of H₂CO molecules. It is seen from Table 5 that the H₂CO destroyed at the surface exceeds its production there, that is H₂CO produced above the surface and transported downwards is also destroyed. The second type of loss due to

Received 21 March; accepted 30 June 1983.

1. Wasserburg, G. J. & Papanastassiou, D. A. in *Essays in Nuclear Astrophysics* (eds Barnes, C. A. et al.) 77 (Cambridge University Press, 1982).
2. Wasserburg, G. J., Papanastassiou, D. A. & Lee, T. in *Les Elements et leurs Isotopes dans l'Univers* (Liege University Press, 1978).
3. Falk, S. W. & Schramm, D. N. *Sky Telescope* **58**, 18 (1979).
4. Bodenheimer, P. *Astrophys. J.* **224**, 488 (1978).
5. Bodenheimer, P. *Fundamental Problems in the Theory of Stellar Evolution, IAU Symp.* No. 93 (1981).
6. Boss, A. P. *Icarus* **51**, 623 (1982).
7. Boss, A. P. *Icarus* (submitted).
8. Agekyan, T. A. & Anosova, Zh. P. *Astr. Zh.* **11**, 1006 (1968).
9. Cameron, A. G. W. *The Moon and the Planets* Vol. 18, 5 (1978).
10. Low, C. & Lynden-Bell, D. *Mon. Not. R. astr. Soc.* **176**, 367 (1976).
11. Larson, R. D. *Mon. Not. R. astr. Soc.* **194**, 809 (1981).
12. Lin, D. N. C. & Papaloizu, J. *Mon. Not. R. astr. Soc.* **191**, 37 (1980).
13. Stahler, S. W., Shu, F. H. & Taam, R. E. *Astrophys. J.* **241**, 637 (1980).
14. Herbig, G. H. *Adv. Astr. Astrophys.* **1**, 47 (1962).
15. Herbig, G. H. in *Spectroscopic Astrophysics* (ed. Herbig, G. H.) 237 (University of California Press, Berkeley, 1970).
16. Jones, B. F. & Herbig, G. H. *Astr. J.* **84**, 1872 (1979).
17. Cohen, M. & Kuhl, L. V. *Astrophys. J. Suppl.* **41**, 743 (1979).
18. Herbig, G. H. *Astrophys. J.* **182**, 129 (1973).
19. Feigelson, E. D. & Kriss, G. A. *Astrophys. J. Lett.* **248**, L35 (1981).
20. Walter, F. M. & Kuhl, L. V. *Astrophys. J.* **250**, 254 (1981).
21. Mundt, R. et al. *Astrophys. J.* (in the press).
22. Appenzeller, I., Chavarria, C., Krautter, J., Mundt, R. & Wolf, B. *Astr. Astrophys.* **90**, 184 (1980).
23. Gahn, G. F., Fredga, K., Liseau, R. & Dravins, D. *Astr. Astrophys.* **73**, L4 (1979).
24. Imhoff, C. L. & Giampapa, M. S. *Astrophys. J. Lett.* **239**, L115 (1980).
25. Giampapa, M. S., Calvet, N., Imhoff, C. L. & Kuhl, L. V. *Astrophys. J.* **251**, 113 (1981).
26. Brown, A., Jordan, C., Millar, T. J., Gondhalekar, P. & Wilson, R. *Nature* **290**, 34 (1981).
27. Kuhl, L. V. *Astr. Astrophys. Suppl.* **15**, 47 (1974).
28. Canuto, V. M., Levine, J. S., Augustsson, T. R. & Imhoff, C. L. *Nature* **296**, 816 (1982).
29. Boesgaard, A. M. & Simon, T. in *SAO Spec. Rep.* No. 392, Vol. II, 161 (1982).
30. Safronov, V. S. *Evolution of the Protoplanetary Cloud and Formation of the Earth and Planets* (NASA TTF-677, 1972).
31. Weidenshilling, S. J. *Icarus* **44**, 172 (1980); **22**, 426 (1974); **27**, 161 (1976).
32. Wetherill, G. W. *A. Rev. Astr. Astrophys.* **18**, 77 (1980).
33. Hayashi, C. in *Fundamental Problems in the Theory of Stellar Evolution, IAU Symp.* No. 93 (1981).
34. Mizuno, H., Nakazawa, K. & Hayashi, C. *Planet. Space Sci.* **30**, 765 (1982).
35. Nakagawa, Y., Nakazawa, K. & Hayashi, C. *Icarus* **45**, 517 (1981).
36. Kaula, W. M. *J. geophys. Res.* **84**, 999 (1979).
37. Elmegreen, B. G. *The Moon and the Planets* **19**, 261 (1978); *Astr. Astrophys.* **80**, 77 (1979).
38. De Campli, W. M. *Astrophys. J.* **244**, 124 (1981).
39. Hartmann, L., Edwards, S. & Avrett, E. *Astrophys. J.* **261**, 279 (1982).
40. Calvet, N., Canto, J. & Rodriguez, L. F. *Astrophys. J.* (in the press).
41. Edwards, S. & Snell, R. L. *Astrophys. J.* **261**, 151 (1982).
42. Stewart, R. W. & Townsend, A. A. *Phil. Trans. R. astr. Soc.* **243**, 48 (1951).
43. Ledoux, P., Schwarzschild, M. & Spiegel, E. *Astrophys. J.* **133**, 184 (1961).
44. Nakano, T., Fukuhima, T., Unno, W. & Kondo, M. *Publ. astr. Soc. Jap.* **31**, 713 (1979).
45. Horedt, G. P., *Astr. Astrophys.* **64**, 173 (1978).
46. Henderson-Sellers, A. & Cogley, J. G. *Nature* **298**, 832 (1982).
47. Wetherill, G. W. *Geochim. cosmochim. Acta. Suppl.* **15**, 1 (1981).
48. Stevenson, D. J. in *Origin and Evolution of the Earth's Earliest Biosphere: An Interdisciplinary Study*, (ed. Schopf, J. W.) (Princeton University Press, in the press).
49. Benlow, A. & Meadows, A. J. *Astrophys. Space Sci.* **46**, 293 (1977).
50. Jakosky, B. M. & Ahrens, T. J. *Proc. 10th Lunar planet. Sci. Conf.* 2727 (1979).
51. Wetherill, G. W. *Proc. 7th Lunar Sci. Conf.* 3245 (1976).
52. Hayashi, C., Nakazawa, K. & Adachi, I. *Publ. astr. Soc. Jap.* **29**, 163 (1977).
53. Thomsen, L. J. *J. geophys. Res.* **85**, 4374 (1980).
54. Kasting, J. F. & Walker, J. C. G. *J. geophys. Res.* **86**, 1147 (1981).
55. Pinto, J. P., Gladstone, G. R. & Yung, Y. L. *Science* **210**, 183 (1980).
56. Levine, J. S. *J. molec. Evol.* **18**, 161 (1982).
57. Levine, J. S., Augustsson, T. R. & Natarajan, M. *Origins Life* **12**, 245 (1982).
58. Ponnampuram, C. in *Origin of Prebiological Systems and Their Molecular Matrices* (ed. Fox, S. W.) 221 (Academic, New York, 1965).
59. Levine, J. S., Augustsson, T. R. & Hoell, J. M. *Geophys. Res. Lett.* **7**, 317 (1980).
60. Ackerman, M. in *Mesospheric Models and Related Experiments* (ed. Fiocco, G.) 149 (Reidel, Dordrecht, 1971).
61. Bar-Nun, A. & Chang, S. J. *J. geophys. Res.* (in the press).

Phosphorylation of isocitrate dehydrogenase as a demonstration of enhanced sensitivity in covalent regulation

David C. LaPorte & Daniel E. Koshland Jr

Department of Biochemistry, University of California, Berkeley, California 94720, USA

The sensitivity to regulation of proteins undergoing covalent modification can be greatly increased when the substrates saturate the converter enzymes. This phenomenon, termed zero-order ultrasensitivity, has been found to occur in the reversible phosphorylation of isocitrate dehydrogenase. The possibility that this enhanced sensitivity is a common feature of covalent regulatory systems is discussed.

REGULATION by covalent modification is known to be involved in the control of almost every type of cellular process^{1,2}. The phosphorylation cycle appears to be the most prevalent, but other types of covalent modification have important roles³. Protein phosphorylation has assumed increasing importance

with the discovery that the gene products of certain oncogenic viruses^{4,5} and various receptor molecules, such as the epidermal growth factor receptor⁶ and the insulin receptor^{7,8}, have kinase activity.

An important feature of any control system is the degree to